

The Mg II and Lyman- α Lines of Nearby K Dwarfs: ISM Components and Flux Measurements¹

Brian E. Wood,² Carol W. Ambruster,³ Alexander Brown,⁴ and Jeffrey L. Linsky²

ABSTRACT

We analyze local ISM absorption observed in the Lyman- α and Mg II h & k lines of six nearby K dwarf stars, using UV spectra of these stars obtained with the Goddard High Resolution Spectrograph on the *Hubble Space Telescope*. For four of the six stars, we detect an absorption component with a velocity and column density consistent with the Local Interstellar Cloud (LIC). For HD 197890, there is no observed component at the expected LIC velocity, or at the projected velocity of the G cloud, which is a nearby cloud in the general direction of the Galactic Center. It also seems doubtful that either of the two components seen toward HD 82558 are LIC or G cloud absorption. The total H I column density toward HD 82558 ($d = 18.3$ pc) is extremely high ($\log N_{\text{H}} = 19.05 \pm 0.15$), representing the largest average H I density detected for any line of sight through the nearby LISM ($n_{\text{H}} \approx 0.2 \text{ cm}^{-3}$). This is particularly remarkable considering that this star is only 39° from the “interstellar tunnel” toward ϵ CMa, where column densities are an order of magnitude lower than this toward stars which are an order of magnitude farther away.

Subject headings: ISM: atoms — stars: chromospheres — stars: late-type — ultraviolet: ISM — ultraviolet: stars

1. Introduction

In 1995–1996, the Goddard High Resolution Spectrograph (GHRS) on board the *Hubble Space Telescope* (HST) observed a selection of six K dwarf stars with spectral types between K0 V and K2 V, all but one of which were also observed by the *Extreme Ultraviolet Explorer* (EUVE). These

¹Based on observations with the NASA/ESA Hubble Space Telescope, obtained at the Space Telescope Science Institute, which is operated by the Association of Universities for Research in Astronomy, Inc. under NASA contract NAS5-26555.

²JILA, University of Colorado and NIST, Boulder, CO 80309-0440; woodb@marmoset.colorado.edu, jlin-sky@jila.colorado.edu.

³Department of Astronomy and Astrophysics, Villanova University, Villanova, PA 19085; ambruster@ucis.vill.edu.

⁴Center for Astrophysics and Space Astronomy, University of Colorado, Boulder, CO 80309-0389; ab@casa.colorado.edu

data were obtained to study how stellar atmospheric structure varies with rotation rate, as the only major characteristic distinguishing these stars is rotation period, which ranges from 0.38 to 6.76 days. Chromospheric and transition region (TR) plasmas ($T < 10^6$ K) produce many emission lines detectable in the UV spectra obtained by GHRS, while EUVE spectra contain many emission line diagnostics of coronal plasma ($T \geq 10^6$ K). Thus, the combination of the two data sets provides a complete picture of how the chromospheric, TR, and coronal plasma emissions vary with rotation for our sample of K dwarfs. Some preliminary results of this study were presented by Ambruster et al. (1998).

In order to derive accurate emission line fluxes from the GHRS and EUVE data, it is necessary to correct for interstellar absorption. The EUVE fluxes are most affected by the ISM because of the H I photoionization edge at 912 Å and the He I photoionization edge at 504 Å, which result in significant continuum absorption in the EUVE bandpasses for even modest ISM column densities (Rumph, Bowyer, & Vennes 1994). In our GHRS data, three of the strongest and most important chromospheric lines show strong absorption features from the local interstellar medium (LISM) — H I Lyman- α at 1216 Å, and the Mg II h & k lines at 2803 Å and 2796 Å, respectively. In this paper, we analyze the interstellar absorption observed in the Lyman- α and Mg II lines of the K dwarfs. In doing so, we hope to measure accurate stellar Lyman- α and Mg II line fluxes after removing the LISM absorption, and also to provide measurements of H I column densities that are crucial for the analysis of the EUVE data.

However, the LISM measurements are also interesting in their own right. Recent studies of Lyman- α , Mg II, and other UV absorption lines have greatly improved our knowledge of the physical properties of the LISM, including measurements of the cosmologically important local D/H ratio (Landsman, Sofia, & Bergeron 1995; Linsky et al. 1995; Dring et al. 1997; Piskunov et al. 1997; Linsky 1998; Sahu et al. 1999), the ionization state of the local cloud (Wood & Linsky 1997; Jenkins et al. 2000), and detections of heliospheric and astrospheric material heated by interactions between the LISM and solar/stellar winds (Linsky & Wood 1996; Wood, Alexander, & Linsky 1996b; Wood & Linsky 1998). High quality UV spectra provided by HST have also been used to construct the first crude three-dimensional models for the distribution of H I in the immediate vicinity of the Sun (Linsky et al. 2000; Redfield & Linsky 2000). The K dwarf spectra, which are all of relatively short lines of sight, will provide more valuable data points for this continuing project.

2. Observations

The six Pleiades Moving Group stars comprising our primary data set are listed in Table 1 together with their spectral types, *Hipparcos* distances (Perryman et al. 1997), Galactic coordinates, and rotation periods. The stars are listed in order of increasing rotation period. In this paper, we also measure the Lyman- α and Mg II fluxes of some other early K dwarfs whose interstellar absorption has been observed by HST and analyzed in the past, and these stars are also listed in Table 1. The references for the spectral types and rotation periods are provided in Table 1. Note,

however, that rotation rates can be slightly variable due to the effects of differential rotation (e.g., Donahue, Saar, & Baliunas 1996; Saar & Osten 1997).

The GHRS observations analyzed in this paper are tabulated in Table 2. A full description of the GHRS instrument is provided by Brandt et al. (1994) and Heap et al. (1995). For each star, the G270M and G160M gratings are used to take moderate resolution spectra ($\Delta\lambda/\lambda \approx 20,000$) of the Mg II h & k and Lyman- α spectral regions, respectively. The observing program includes observations of other spectral regions, but we will focus here only on the spectra of Lyman- α and Mg II.

The spectra listed in Table 2 were taken through the small science aperture (SSA) to maximize the spectral resolution and, more importantly for the Lyman- α spectrum, to minimize the amount of geocoronal Lyman- α emission. For all of our Lyman- α data, the geocoronal emission feature (when visible at all) is well within the core of the broad, saturated LISM absorption line. This makes it easy to remove, which we do by fitting a Gaussian to the feature and then subtracting the Gaussian from the data. Each spectrum was taken in four sequential readouts using the FP-SPLIT option, in which the spectrum is dithered on the detector to allow a better correction for fixed pattern noise (Heap et al. 1995). The data were reduced using the IDL-based CALHRS software developed by the GHRS team (Robinson et al. 1992).

The last column of Table 2 indicates whether or not a special wavelength calibration observation of the Pt calibration lamp was taken along with the observation to allow for a more accurate wavelength calibration. When such an observation is available, we use it to determine a better zero-point offset correction for the wavelengths of the associated science spectrum. When such an observation is not available, an offset correction is provided by the so-called SPYBAL (“spectrum y-balance”) observations of the calibration lamp. The SPYBALs are used to properly center spectra on the diode array, and are taken with the same grating as the accompanying science observation, but generally of a different spectral region. Soderblom, Sherbert, & Hulbert (1993) describe how the SPYBALs can also be used to provide offset corrections for the wavelengths of science observations. Even with these corrections, we do not expect the uncertainties in the wavelength scales of our SPYBAL-calibrated spectra to be lower than about $\pm 3 \text{ km s}^{-1}$.

3. Analyzing the Interstellar Absorption

3.1. Modelling the Mg II Line Profiles

Figure 1 shows the Mg II h & k lines observed from the K dwarfs. The rest wavelengths in air of the h & k lines are 2802.705 Å and 2795.528 Å, respectively. Interstellar absorption is clearly seen contaminating both lines, with the stronger absorption in the k line due to a larger oscillator absorption strength for that line. In Figure 2, the Mg II h lines are displayed on a heliocentric velocity scale, along with our best fits to the interstellar absorption, which we now discuss in detail.

The resolution of these G270M observations is not sufficient to fully resolve the LISM absorption. This makes it difficult to identify the number of LISM components, and in some cases also makes it difficult to separate the LISM absorption from the intrinsic line profile. Previously observed slowly rotating K dwarfs have Mg II profiles with self-reversals, i.e., the profiles are double-peaked (Linsky & Wood 1996; Wood & Linsky 1998). For HD 82558, HD 82443, and HD 17925 it is difficult to tell how much of the apparent absorption is actually interstellar and how much of it is just due to a self-reversal of the stellar line profile, although analyzing the h and k lines together helps to solve this problem since the relative depth of the possible self-reversals should be about the same for both lines, while the depth of LISM absorption should be larger for the k line.

We initially tried using Gaussians to model the Mg II profiles of HD 82443. The location of the observed absorption feature is such that it is clearly associated with the Local Interstellar Cloud (see below), but when the intrinsic stellar line profiles are assumed to be Gaussian, the Doppler parameter we measure for the LISM absorption is significantly larger than is typically found for this cloud, and when the h and k lines are fitted separately, the k line column density is somewhat smaller than that of the h line. Both of these properties suggest that Gaussians overestimate the amount of flux overlying the LISM absorption. Thus, we experimented with profiles with self-reversals of various depths, which were created manually, point-by-point. In our best fit shown in Figure 2, the stellar profile has only a very weak self-reversal.

The Mg II lines of HD 17925 proved to be the hardest to model. The analysis was similar to that described above for HD 82443, but the apparent existence of two LISM components (see below) and the greater depth of the absorption make the HD 17925 analysis more difficult and therefore more uncertain. Nonetheless, we believe that the Mg II lines of HD 17925 do have self-reversals. However, the HD 17925 profile shown in Figure 2 has a very strange property — the red peak is stronger than the blue peak. To the best of our knowledge, all other self-reversed Mg II line profiles observed from cool main sequence stars have stronger *blue* peaks (Wood et al. 1996a; Linsky & Wood 1996; Wood & Linsky 1998), as is also apparently the case for HD 82443.

We cannot completely rule out the possibility that this is just a manifestation of the difficulty in separating the LISM absorption and self-reversal of HD 17925’s Mg II lines. However, a more likely explanation is that HD 17925 is actually a binary star, with Mg II emission from an unresolved secondary star being responsible for the stronger red peak. Support for this assertion comes from observations of HD 17925’s photospheric absorption lines, which have variable widths that also suggest the presence of a companion star (Henry, Fekel, & Hall 1995; Fekel 1997).

Rotational broadening is so severe for HD 197890 that the narrow absorption seen near the center of its Mg II lines is obviously entirely interstellar, and for HD 1405 and HD 220140 the absorption is located far enough from the center of the line that it is also clearly interstellar. Thus, for these stars we can estimate the stellar line profile simply by interpolating over the absorption, which we do by performing a polynomial fit to data points on both sides of the absorption.

The Mg II lines of HD 1405 and HD 220140 clearly do not have self-reversals. This could

be due in part to rotational smearing. However, since these stars are very active it might also be a stellar manifestation of a property of solar Mg II lines observed from active regions, where the depth of the self-reversals tends to be less than than observed in quiet solar regions (Doschek & Feldman 1977). In any case, HD 82558 is rotating even faster than HD 1405 and HD 220140, and is at least as active as these stars, so it is reasonable to presume that the Mg II lines of HD 82258 also do not possess self-reversals. Thus, for HD 82558 we use Gaussian fits to estimate the profiles of the Mg II lines (see Fig. 2).

3.2. Fitting the Interstellar Mg II Lines

Once the stellar Mg II profiles have been estimated, we fit the LISM absorption using standard techniques. The atomic parameters needed for this procedure are taken from Morton (1991). We use Voigt functions to represent the opacity profiles of the fitted absorption. Before being compared with the data, the absorption profile is convolved with the line spread function appropriate for SSA GHRS observations, which we assume to be a Gaussian with a width of 3.7 pixels (Gilliland 1994). In Figure 2, dotted lines show the absorption components before convolution, and thick solid lines that fit the data show the absorption after correcting for instrumental broadening.

For each absorption component there are three parameters: the central velocity (V_{Mg}), the column density (N_{Mg}), and the Doppler parameter (b_{Mg}). The Doppler parameter is related to the temperature (T) and nonthermal velocity (ξ) of the interstellar material by the equation $b^2 = 0.0165T/A + \xi^2$, where b has units of km s^{-1} and A is the atomic weight of the element in question ($A = 24$ for Mg). Columns 3–5 of Table 3 list the parameters for the Mg II fits. Before deciding on these final fit parameters and their uncertainties, we tried fitting the h & k lines both independently and simultaneously to see how the parameters change. This gives us an idea of the magnitude of the systematic errors involved in the fits, allowing us to more accurately estimate the uncertainties in the various fit parameters. Note that these are just measurement uncertainties and do not include possible errors in the wavelength calibrations (see §2).

In the heliocentric rest frame, the Local Interstellar Cloud (LIC) in which the Sun is embedded is flowing toward Galactic coordinates $l = 186^\circ$ and $b = -16^\circ$ at a velocity of about 25.7 km s^{-1} (Witte et al. 1993; Lallement et al. 1995). Using this vector we compute the projected LIC velocities, $V(\text{LIC})$, for the lines of sight toward our K dwarfs. These velocities are listed in the second column of Table 4 and can be compared with the measured V_{Mg} velocities in Table 3 to identify which components are from LIC material.

For most lines of sight we expect to detect absorption at the expected LIC velocity. However, the Sun is less than 0.2 pc from the edge of the LIC in the general direction of the Galactic Center (Wood, Linsky, & Zank 2000). For lines of sight in this direction LIC absorption is often not observed, but absorption from a different cloud called the “G cloud” is generally detected. The G cloud also has an accurately measured vector with a direction similar to that of the LIC ($l = 186^\circ$,

$b = -16^\circ$), but with a slightly faster speed of 29.4 km s^{-1} (Lallement & Bertin 1992). In column 3 of Table 4 we list the velocities, $V(G)$, expected for G cloud material for our studied lines of sight.

For HD 220140 and HD 82443, the Mg II lines can be fitted with only one LISM absorption component, which has a velocity consistent with the LIC (see Fig. 2 and Table 3). Previous analyses of LIC and G cloud Mg II absorption lines observed with high spectral resolution have found that the Doppler parameters are typically in the range $b_{\text{Mg}} = 2.2 - 3.5 \text{ km s}^{-1}$ (Linsky & Wood 1996; Dring et al. 1997; Piskunov et al. 1997; Wood & Linsky 1998; Wood et al. 2000), and the b_{Mg} values reported for HD 220140 and HD 82443 in Table 3 fall nicely within this range.

The Mg II absorption seen toward the other four stars cannot be modeled with only one component. Thus, for these stars we model the absorption with two components, although the limited resolution of our data means that even more components could be present. For HD 197890 the need for two components is obvious since the components are well separated (see Fig. 2). For HD 82558, HD 1405, and HD 17925, the evidence for the existence of two components is more subtle. When the absorption seen toward these stars is fitted with only one component, the central velocity is consistent with neither $V(\text{LIC})$ nor $V(G)$, and the Doppler parameter is very large ($b_{\text{Mg}} > 5 \text{ km s}^{-1}$). However, in the two component fits one of the components does lie at the expected LIC velocity, and the Doppler parameters are within the expected range. Thus, we consider the two component models presented in Figure 2 and Table 3 to be our best interpretations of the data. However, because the components are so highly blended, it was necessary to reduce the number of free parameters of these fits, so we have forced the Doppler parameters of the two components to be the same. This is indicated in Table 3 by the use of parentheses around the b_{Mg} values of the second component.

The second column of Table 3 indicates which components are identified with LIC absorption. The velocity of HD 82558’s Component 1 is consistent with both the LIC and G clouds, but it is very difficult to associate it with either for reasons that will become clear after the Lyman- α lines are analyzed (see §3.3). For the multicomponent fits, we have included a line in Table 3 in which total column densities are listed. Note that for the highly blended components, the total Mg II column density can be computed more accurately than the column densities of the individual components.

Only one of our stars lies anywhere near the Galactic Center direction: HD 197890, with $l = 6^\circ$ and $b = -38^\circ$. For this line of sight we would have *a priori* expected to see G cloud absorption but no LIC absorption. The $V(\text{LIC})$ and $V(G)$ values in Table 4 are about the same ($V(\text{LIC}) = -14.9 \text{ km s}^{-1}$ and $V(G) = -15.2 \text{ km s}^{-1}$). However, the V_{Mg} values listed in Table 3 for the two components are $V_{\text{Mg}} = -23 \pm 2 \text{ km s}^{-1}$ and $V_{\text{Mg}} = 0 \pm 1 \text{ km s}^{-1}$, inconsistent with both the LIC and G clouds. We cannot rule out the possibility that Component 1 is actually an unresolved combination of two components. The b_{Mg} value for Component 1 is indeed suspiciously high, although with a large uncertainty ($b_{\text{Mg}} = 4.4 \pm 1.4 \text{ km s}^{-1}$). However, the $V(\text{LIC})$ and $V(G)$ velocities lie at the very red edge of the observed Component 1 absorption (see Fig. 2), meaning

that the LIC and G clouds cannot account for a significant amount of this absorption.

In order to confirm this finding, we processed archival GHRS Mg II observations of AU Mic, an M0 V star 9.94 pc from the Sun and only 5° from HD 197890. The AU Mic Mg II h line spectrum is compared with the HD 197890 data in Figure 3. The AU Mic spectrum was taken with the Ech-B grating and therefore has a higher resolution than the G270M HD 197890 spectrum, but it was observed through the large science aperture (LSA) prior to the installation of the COSTAR corrective optics into HST, meaning the resolution is significantly degraded relative to post-COSTAR Ech-B data (Heap et al. 1995).

Only one LISM absorption component is seen toward AU Mic, corresponding to Component 1 seen toward HD 197890, although we had to arbitrarily shift the AU Mic spectrum by -1 km s^{-1} to make the absorption line up perfectly. Such a shift is within the combined uncertainties of the wavelength calibrations of the two Mg II spectra. A difference in the projected cloud velocity between the two stars might also contribute to the slight velocity difference, even though the stars are only 5° apart.

The fit to the HD 197890 Mg II h line in Figure 2 is reproduced in Figure 3, and we also compare the Component 1 absorption component with the AU Mic data, where we have used a line spread function appropriate for pre-COSTAR LSA Ech-B data to correct for instrumental smoothing (Gilliland & Hulbert 1993). The reasonably good fit to the AU Mic data demonstrates that the Component 1 cloud does not extend beyond AU Mic’s 9.94 pc distance. Otherwise we would see more absorption from the cloud toward HD 197890, which lies 44.4 pc away. The Component 2 cloud, on the other hand, must lie beyond AU Mic, since no Component 2 absorption is seen in the AU Mic spectrum.

The dashed lines in Figure 3 show the expected location of G cloud absorption, with the predicted LIC absorption being at about the same velocity. As mentioned above, the LIC and G clouds are clearly not significant contributors to the Component 1 absorption. Thus, neither the LIC nor the G cloud is detectable toward HD 197890 or AU Mic. The non-detection of the LIC is expected (see above), but the absence of G cloud absorption is somewhat surprising. Apparently the G cloud does not extend very far to southern Galactic latitudes, explaining why it is not seen toward either HD 197890 ($b = -38^\circ$) or AU Mic ($b = -37^\circ$). We estimate an upper limit of $\log N_{\text{Mg}} < 12.0$ for the LIC and G clouds along this line of sight. Based on previous measurements of the Mg II/H I ratio in the LIC and G clouds (Dring et al. 1997; Piskunov et al. 1997; Wood & Linsky 1998; Wood et al. 2000), this corresponds to upper limits for hydrogen of $\log N_{\text{H}} < 17.5$ for the LIC and $\log N_{\text{H}} < 16.8$ for the G cloud.

3.3. The Lyman- α Lines

The Lyman- α lines of the six K dwarfs are displayed in Figure 4. The stellar emission lines are contaminated by broad interstellar H I absorption centered at a rest wavelength of 1215.670 Å,

and weaker deuterium (D I) absorption 0.33 Å blueward of the H I absorption. The figure also shows our best estimates for the shapes of the uncontaminated stellar Lyman- α lines, and our best fits to the LISM absorption, which are discussed in detail below. The H I fit parameters are listed in columns 6–8 of Table 3.

The opacity of interstellar Lyman- α is so large that the H I absorption has wings that extend well beyond the saturated core of the absorption. When a value for the interstellar H I column density (N_{H}) is assumed, the shape of the wings of the intrinsic stellar line profile outside the saturated core can be computed simply by extrapolating upwards from the data, by multiplying the observed flux by $\exp(\tau_{\lambda})$. The shape of the center of the stellar line profile can then be estimated by extrapolating between the wings, using the observed shapes of the Mg II lines as models for the appearance of Lyman- α . In this way, we create a set of model stellar Lyman- α profiles designed to produce fits to the absorption for a set of assumed values for N_{H} . We can then perform fits to the H I and D I absorption lines using these profiles to see which ones actually yield good fits to the data.

We have used this procedure for analyzing Lyman- α lines many times (Linsky & Wood 1996; Piskunov et al. 1997; Wood & Linsky 1998; Wood et al. 2000). The analysis described in Piskunov et al. (1997) is particularly relevant, especially for the three lines of sight discussed in that paper based on moderate resolution HST observations of Lyman- α (31 Com, β Cet, and β Cas), such as we have here. The justification for the use of the Mg II lines in estimating the shape of the Lyman- α profiles is that Mg II h & k and Lyman- α are all highly optically thick chromospheric lines that have similar appearances in solar spectra.

One of the main goals of the previous analyses mentioned above was the measurement of the local D/H ratio. However, it would be very difficult to accurately measure D/H for our data because of the modest spectral resolution, the relatively low signal-to-noise of the data, and the existence of multiple LISM components for all but two of our stars. Thus, in our analysis we simply assume $\text{D}/\text{H} = 1.5 \times 10^{-5}$, which is the measured value for the LIC. There is as yet no conclusive evidence that D/H differs significantly from this value anywhere within the 50 pc distance range of our sample of stars (Linsky 1998). The assumption of a D/H value means the observed D I absorption constrains the H I column density as well as the D I column density, which is very helpful.

As usual in Lyman- α analyses we assume H I and D I have the same centroid velocities, and we assume the H I and D I Doppler parameters are related by $b_{\text{D}} = b_{\text{H}}/2^{1/2}$. This relation is applicable if nonthermal velocities are negligible compared to the thermal velocities of H I and D I, which previous work has demonstrated to be a reasonably good approximation for the warm LISM gas (Linsky & Wood 1996; Piskunov et al. 1997; Wood & Linsky 1998; Wood et al. 2000). We take the fine structure of the H I and D I Lyman- α lines into account in the analysis, although this has little effect on our results since the two fine structure components are separated by only 1.3 km s $^{-1}$. With the assumptions mentioned above the D I parameters are entirely constrained by the H I parameters, so the D I parameters are not listed in Table 3.

In the case of multi-component fits, additional assumptions must be made to limit the number of free fit parameters and ensure a unique fit to the data. For the two-component fits in Figure 4, we assume the velocity separation of the components is the same as measured in the Mg II fits. We also assume the Doppler parameters of both components are identical, and that the Mg II/H I abundance ratio is the same for both components. This last assumption is potentially the most questionable since Mg II/H I and Mg II/D I ratios are known to vary quite a bit in the LISM (Piskunov et al. 1997). Thus, the column densities of the individual components listed in Table 3 could be more uncertain than indicated by the quoted error bars, but the *total* H I column densities should not be greatly sensitive to this assumption. With the constraints listed above, the parameters of the second component are completely constrained by those of the first. This interdependence is indicated in Table 3 by the use of parentheses around the fit parameters of second components in two component fits.

With all the assumptions listed above, each fit in Figure 4 actually has only three free parameters. By experimenting with fits computed using various stellar line profile models, we collect a set of acceptable fits to the data that we use to define the fit parameters and uncertainties listed in Table 3. The measured H I velocities, V_H , are found to be consistent with the Mg II velocities, V_{Mg} , considering the quoted measurement uncertainties and the uncertainties in the wavelength calibrations of the spectra (see §2).

In many previous analyses of high resolution Lyman- α spectra, the LISM H I absorption has been found to be blended with absorption from heliospheric material around the Sun and/or astrospheric material surrounding the observed star (Linsky & Wood 1996; Wood et al. 1996b; Dring et al. 1997; Wood & Linsky 1998; Wood et al. 2000). The lower quality of our data makes it difficult to search for such absorption, but the two spectra most likely to show evidence for this additional absorption are the ones with the lowest H I column densities: HD 220140 and HD 82443. Although we do not try to model these two data sets with heliospheric or astrospheric absorption, we note that the Lyman- α fits for these two stars do have some undesirable properties that might indicate the presence of this extra absorption.

The fit to the D I line of HD 82443 in Figure 4 is not particularly good and suggests that H I may actually be redshifted relative to D I. Models suggest that heliospheric H I absorption should be redshifted relative to the LIC absorption for all lines of sight through the heliosphere (Baranov, Izmodenov, & Malama 1998; Müller, Zank, & Lipatov 2000), so it is possible that heliospheric H I is contributing to the Lyman- α absorption on the red side of the line, thereby inducing the apparent redshift of H I relative to D I.

For HD 220140, the observed D I absorption appears to be somewhat narrower than the fit. Also, the measured H I Doppler parameter is very high ($b_H = 14.2 \pm 0.5 \text{ km s}^{-1}$), suggesting a very hot LIC temperature of $T = 12,200 \pm 800 \text{ K}$. Previous measurements of the LIC temperature based on much higher quality data suggest temperatures no higher than about 9500 K, and more typically in the 7000 – 9000 K range (Linsky et al. 1995; Dring et al. 1997; Piskunov et al. 1997;

Wood & Linsky 1998). Both of these properties could in principle be explained by the broadening of the H I Lyman- α absorption line by heliospheric and/or astrospheric absorption, which results in overestimates of b_{H} and b_{D} .

For the two component fits, we list total H I column densities in Table 3 in addition to the individual component values, as is also done for Mg II. The total N_{H} values observed for each line of sight will prove useful in analyzing the EUVE observations of the stars (see §1). In the last column of Table 3, the total Mg II and H I column densities are used to derive logarithmic Mg depletion values for the six lines of sight, where $D(\text{Mg}) \equiv \log(N_{\text{Mg}}/N_{\text{H}}) - \log(\text{Mg}/\text{H})_{\odot}$. The solar Mg/H ratio is 3.9×10^{-5} (Anders & Grevesse 1989). We do not list $D(\text{Mg})$ values for the individual components of the two-component fits since the Mg II/H I abundance ratio was assumed to be the same for both components in the H I fits.

For the single component HD 220140 and HD 82443 lines of sight, which both sample the LIC and only the LIC, our measured Mg depletions ($D(\text{Mg}) = -0.84 \pm 0.14$ and $D(\text{Mg}) = -0.89 \pm 0.18$, respectively) are reasonably close to previous LIC measurements based on high resolution HST spectra, which typically show $D(\text{Mg}) \approx -1.1$ (Dring et al. 1997; Piskunov et al. 1997; Wood & Linsky 1998). For the HD 1405 and HD 17925 lines of sight, which have second components in addition to the LIC component, $D(\text{Mg}) = -0.54 \pm 0.32$. We propose that the second components observed for these two lines of sight have less Mg depletion than the LIC, resulting in these lower depletion values.

Redfield & Linsky (2000) collected measurements of LIC H I column densities for many lines of sight and used them to construct a three dimensional model of the LIC. In the last column of Table 4 we list the LIC column densities predicted by this model for our six lines of sight. For HD 1405, HD 220140, HD 82443, and HD 17925 these predictions agree surprisingly well with the measured LIC column densities listed in Table 3, providing support for the accuracy of the model. For HD 197890 there is no detected LIC component, as discussed in §3.2, and the very low predicted LIC column density in Table 4 is consistent with this result. For HD 82558, there is a component close to the expected LIC velocity, but the measured column density ($\log N_{\text{H}} = 18.75 \pm 0.15$) is almost two orders of magnitude larger than the prediction ($\log N_{\text{H}}(\text{LIC}) = 16.89$).

While some inaccuracies in the Redfield & Linsky (2000) model are to be expected, the HD 82558 discrepancy is extreme. If HD 82558’s Component 1 is in fact the LIC, it would suggest the existence of a small dense knot of material within the LIC or a very extended, narrow finger of material along the HD 82558 line of sight. Another possibility is that it is actually G cloud material. The $V(\text{G})$ velocity listed for HD 82558 in Table 4 does in fact agree with the Component 1 V_{Mg} and V_{H} velocities better than the $V(\text{LIC})$ velocity does. Furthermore, although the G cloud is believed to lie mainly toward the Galactic Center, crude sketches of the cloud’s location from Lallement & Bertin (1992), Lallement et al. (1995), and Wood et al. (2000) suggest that the cloud could extend to the $l = 245^\circ$ longitude of HD 82558.

Unfortunately, the $D(\text{Mg}) = -1.44 \pm 0.21$ value measured toward HD 82558 is much closer

to typical LIC values (see above) than to the $D(\text{Mg}) \approx -0.4$ values previously measured for the G cloud (Piskunov et al. 1997; Wood et al. 2000). If the HD 82558 Component 1 is in fact the G cloud, it would suggest that Mg depletions must vary greatly within the cloud. Perhaps the most likely interpretation of Component 1 is that it is neither the LIC nor the G cloud, but is an entirely different cloud with the same projected velocity. The two clouds seen toward HD 82558 must be quite dense and compact to account for such high column densities.

The $\log N_{\text{H}} = 19.05 \pm 0.15$ column density observed toward HD 82558 implies an average H I density along this line of sight of $n_{\text{H}} \approx 0.20 \text{ cm}^{-3}$. *We believe that this is the highest average density ever observed for any line of sight through the nearby LISM*, which strengthens the argument that the absorption toward HD 82558 is from neither the LIC nor the G cloud. The high column density is clearly evident just by looking at HD 82558’s Lyman- α line in Figure 4. The H I absorption is so broad that it is blended with the D I absorption. A high column density is also indicated by the absence of any detected emission in the EUVE MW (170–380 Å) spectrum of this star.

By comparison, the column density observed toward HD 82443 is quite small ($\log N_{\text{H}} = 17.70 \pm 0.15$), despite the fact that HD 82443 and HD 82558 are both 18 pc away and the two stars are only 39° apart in the sky. Perhaps even more impressive is that HD 82558 is also only 39° from the “interstellar tunnel” toward ϵ CMa ($l = 240^\circ$, $b = -11^\circ$), for which ISM column densities are lower than $\log N_{\text{H}} = 18.0$ even for lines of sight as long as 200 pc (Gry et al. 1995; Vallerga & Welsh 1995). In the future, it would be interesting to sample other lines of sight near HD 82558 to determine the angular extent to which the high column densities persist.

3.4. Chromospheric Line Fluxes

Now that stellar Mg II and Lyman- α profiles have been estimated for the purpose of analyzing the LISM absorption, we can also measure the fluxes of those Mg II and Lyman- α profiles. We measure these fluxes by direct integration, and the results are tabulated in Table 5. As mentioned in §2, many previous analyses of LISM Mg II and Lyman- α absorption features have also utilized K dwarf spectra obtained by HST. However, stellar line fluxes have generally not been reported in the literature since these studies were focused on the properties of the LISM.

Therefore, in addition to the line fluxes of the six stars analyzed here, we take this opportunity to list in Table 5 the Mg II and/or Lyman- α line fluxes for seven previously analyzed K0–K5 dwarf stars. References for the interstellar Mg II/Lyman- α absorption analyses of these lines of sight are provided in the last column of Table 5. The inclusion of the additional fluxes in Table 5 is potentially very useful for studies of the K dwarf rotation-activity relation because it extends the sample to longer rotation periods than our six star sample by itself (see Table 1).

Estimated uncertainties for the Mg II and Lyman- α fluxes are listed in Table 5 in the form of percent errors. In §3.3 we described how uncertainties in the Lyman- α LISM parameters were derived by experimenting with different stellar profiles. The uncertainties in the stellar Lyman- α

fluxes are also estimated in this process. As Table 5 suggests, uncertainties of 20–25% are typical for the Lyman- α fluxes. For HD 197890, the uncertainty is a bit lower (15%) because the very large width of this star’s Lyman- α line makes it easier to interpolate over the LISM absorption (see Fig. 4). A lower 15% uncertainty is also quoted for HD 26965 because for this star more of the stellar profile is uncontaminated by LISM absorption due to a large velocity separation between the stellar emission and LISM absorption (see Wood & Linsky 1998). For HD 82558, the Lyman- α flux uncertainty is quite large (40%) because the very high column density of this line of sight absorbs a larger percentage of the star’s total line emission (see Fig. 4).

The uncertainty in the Mg II fluxes is not generally dominated by the uncertainty in the ISM correction, but by the uncertainties in the extent of the emission line. The Mg II lines lie on top of a photospheric continuum, the shape of which is unknown because of the overlying chromospheric emission. However, it is likely that the photospheric continuum is close to zero underneath much of the chromospheric line because of absorption from Mg II ions in the photosphere and lower chromosphere (Linsky & Ayres 1978; Wood et al. 1996a). Thus, in calculating the chromospheric Mg II fluxes we assume no underlying photospheric continuum. Inaccuracies in this assumption and uncertainties in the wavelength range used to compute the emission line flux are the major sources of systematic error in the flux measurements. For early K stars the photospheric flux level around 2800 Å is fairly low (see Fig. 1), but we believe it still results in uncertainties of a few percent. For a few stars, especially HD 17925, the LISM correction further increases the estimated Mg II flux uncertainty (see Table 5).

4. Summary

We have presented HST/GHRS observations of six K dwarf stars, and have analyzed the interstellar absorption seen in the Lyman- α and Mg II h & k lines of these stars. Having measured the properties of the LISM absorption components seen in these data and measured stellar Lyman- α and Mg II fluxes corrected for this absorption, we summarize our primary results as follows:

1. One of our stars, HD 17925, has Mg II lines that appear to have double-peaked Mg II lines with stronger red peaks than blue peaks. This is very unusual since the Mg II lines of cool main sequence stars generally have stronger blue peaks. Although we cannot rule out the possibility that this is due to difficulties in removing the LISM absorption, we think it is more likely that emission from a companion star is contributing to the lines.
2. For four of the six stars (HD 1405, HD 220140, HD 82443, and HD 17925), a LISM component is identified that not only has a velocity consistent with the projected velocity of the LIC, but also has an H I column density in excellent agreement with the predictions of the Redfield & Linsky (2000) model of the LIC. This result provides support for the accuracy of the column densities predicted by this LIC model.

3. Neither LIC nor G cloud absorption is observed toward HD 197890. Based on the direction of this line of sight, the LIC nondetection was expected (e.g., Redfield & Linsky 2000), but the G cloud nondetection is somewhat surprising, and indicates that the G cloud does not extend to Galactic latitudes as far south as HD 197890 ($b = -38^\circ$). This result was confirmed using GHRS Mg II observations of AU Mic, a star only 5° from HD 197890.
4. Two LISM components are detected toward HD 82558, and one has a velocity close to both the LIC and G cloud velocities. However, it is very difficult to associate the component with either the LIC or G clouds, mostly because of its extremely high column density. The total H I column density toward HD 82558 is $\log N_{\text{H}} = 19.05 \pm 0.15$. The implied average density along this 18.3 pc line of sight, $n_{\text{H}} \approx 0.2 \text{ cm}^{-3}$, is the largest such density measured from HST data for any line of sight through the nearby LISM. Interestingly enough, the star lies only 39° from ϵ CMa, a direction where column densities are notoriously low — $\log N_{\text{H}} \leq 18.0$ for lines of sight as long as 200 pc.
5. In addition to the six stars analyzed here, we also measure Lyman- α and/or Mg II fluxes for seven other K stars based on previously published LISM absorption analyses. The line fluxes for the stars in this expanded data set promise to be very useful for studying the chromospheric rotation-activity relation of K dwarf stars.

We would like to thank F. Fekel for providing us with new spectral type measurements of HD 197890 and HD 82558, and we would like to thank the referee, S. Federman, for many useful comments. We also thank NASA for support under grant S-56500-D to the University of Colorado and NIST.

REFERENCES

- Ambruster, C. W., Brown, A., Fekel, F. C., Harper, G. M., Fabian, D., Wood, B. E., & Guinan, E. F. 1998, in *Cool Stars, Stellar Systems, and the Sun*, Tenth Cambridge Workshop, ed. R. A. Donahue & J. A. Bookbinder (San Francisco: ASP), 1205
- Anders, E., & Grevesse, N. 1989, *Geochim. Cosmochim. Acta*, 53, 197
- Baranov, V. B., Izmodenov, V. V., & Malama, Y. G. 1998, *J. Geophys. Res.*, 103, 9575
- Bianchi, L., Jurcsik, J., & Fekel, F. C. 1991, *A&A*, 245, 604
- Brandt, J. C., et al. 2000, *AJ*, in preparation
- Brandt, J. C., et al. 1994, *PASP*, 106, 890
- Cutispoto, G., Kürster, M., Pagano, I., & Rodonò, M. 1997, *IBVS*, No. 4419
- Donahue, R. A., Saar, S. H., & Baliunas, S. L. 1996, *ApJ*, 466, 384
- Doschek, G. A., & Feldman, U. 1977, *ApJS*, 35, 471
- Dring, A. R., Linsky, J. L., Murthy, J., Henry, R. C., Moos, W., Vidal-Madjar, A., Audouze, J., & Landsman, W. 1997, *ApJ*, 488, 760
- Fekel, F. C. 1997, *PASP*, 109, 514
- Fekel, F. C., Bopp, B. W., Africano, J. L., Goodrich, B. D., Palmer, L. H., Quigley, R., & Simon, T. 1986, *AJ*, 92, 1150
- Gilliland, R. L. 1994, *GHRS Instrument Science Report 063* (Baltimore: STScI)
- Gilliland, R. L., & Hulbert, S. J. 1993, *GHRS Instrument Science Report 055* (Baltimore: STScI)
- Gliese, W. & Jahreiss, H. 1991, *Third Catalogue of Nearby Stars* (Veröffentlichungen des Astronomischen Rechen-Instituts, University of Heidelberg)
- Gry, C., Lemonon, L., Vidal-Madjar, A., Lemoine, M., & Ferlet, R. 1995, *A&A*, 302, 497
- Heap, S. R., et al. 1995, *PASP*, 107, 871
- Henry, G. W., Fekel, F. C., & Hall, D. S. 1995, *AJ*, 110, 2926
- Hooten, J. T., & Hall, D. S. 1990, *ApJS*, 74, 225
- Innis, J. L., Thompson, K., Coates, D. W., & Lloyd Evans, T. 1988, *MNRAS*, 235, 1411
- Jenkins, E. B., et al. 2000, *ApJ*, in press
- Jetsu, L. 1993, *A&A*, 276, 345

- Lallement, R., & Bertin, P. 1992, *A&A*, 266, 479
- Lallement, R., Ferlet, R., Lagrange, A. M., Lemoine, M., & Vidal-Madjar, A. 1995, *A&A*, 304, 461
- Landsman, W., Sofia, U. J., & Bergeron, P. 1995, in *Science with the Hubble Space Telescope II*, ed. P. Benvenuti, F. Macchetto, & E. Schreier (Paris: ESA), 454
- Linsky, J. L. 1998, *Space Sci. Rev.*, 84, 285
- Linsky, J. L., & Ayres, T. R. 1978, *ApJ*, 220, 619
- Linsky, J. L., Diplas, A., Wood, B. E., Brown, A., Ayres, T. R., & Savage, B. D. 1995, *ApJ*, 451, 335
- Linsky, J. L., Redfield, S., Wood, B. E., & Piskunov, N. 2000, *ApJ*, 528, 756
- Linsky, J. L., & Wood, B. E. 1996, *ApJ*, 463, 254
- Mantegazza, L., Poretti, E., Antonello, E., & Bossi, M. 1992, *A&A*, 256, 459
- Messina, S., Guinan, E. F., Lanza, A. F., & Ambruster, C. 1999, *A&A*, 347, 249
- Morton, D. C. 1991, *ApJS*, 77, 119
- Müller, H. -R., Zank, G. P., & Lipatov, A. S. 2000, *J. Geophys. Res.*, submitted
- Perryman, M. A. C., et al. 1997, *A&A*, 323, L49
- Piskunov, N., Wood, B. E., Linsky, J. L., Dempsey, R. C., & Ayres, T. R. 1997, *ApJ*, 474, 315
- Redfield, S., & Linsky, J. L. 2000, *ApJ*, to appear May 10
- Robinson, R. D., Blackwell, J., Feggans, K., Lindler, D., Norman, D., & Shore, S. N. 1992, *A User's Guide to the GHRS Software, Version 2.0* (Greenbelt: Goddard Space Flight Center)
- Rumph, T., Bowyer, S., & Vennes, S. 1994, *AJ*, 107, 2108
- Saar, S. H., & Osten, R. A. 1997, *MNRAS*, 284, 803
- Sahu, M. S., et al. 1999, *ApJ*, 523, L159
- Soderblom, D. R., Sherbert, L. E., & Hulbert, S. J. 1993, *GHRS Instrument Science Report 053* (Baltimore: STScI)
- Vallerga, J. V., & Welsh, B. Y. 1995, *ApJ*, 444, 702
- Wichmann, R., Bastian, U., Krautter, J., Jankovics, I., & Ruciński, S. M. 1998, *MNRAS*, 301, L39
- Witte, M., Rosenbauer, H., Banaszkewicz, M., & Fahr, H. 1993, *Adv. Space Res.*, 13, 121

- Wood, B. E., Alexander, W. R., & Linsky, J. L. 1996b, ApJ, 470, 1159
- Wood, B. E., Harper, G. M., Linsky, J. L., & Dempsey, R. C. 1996a, ApJ, 458, 761
- Wood, B. E., & Linsky, J. L. 1997, ApJ, 474, L39
- Wood, B. E., & Linsky, J. L. 1998, ApJ, 492, 788
- Wood, B. E., Linsky, J. L., & Zank, G. P. 2000, ApJ, to appear July 1

Table 1. List of K Dwarfs

Star	Alternate Name	Spectral Type	d (pc)	l (deg)	b (deg)	P_{rot} (days)	References
Primary Sample							
HD 197890	“Speedy Mic”	K2-3 V	44.4	6	−38	0.38	1,2
HD 82558	LQ Hya	K2 V	18.3	245	28	1.60	3,4
HD 1405	PW And	K2 V	21.9	115	−31	1.75	1,5
HD 220140	V368 Cep	K2 V	19.7	119	17	2.77	6,7
HD 82443	DX Leo	K0 V	17.7	201	46	5.38	8,9
HD 17925	EP Eri	K2 V	10.4	192	−58	6.76	8,10
Additional Stars							
HD 36705	AB Dor	K1 V	14.9	275	−33	0.51	11,12
HD 22049	ϵ Eri	K2 V	3.22	196	−48	11.7	10,13
HD 155886	36 Oph A	K1 V	5.46	358	7	20.7	10,13
HD 209100	ϵ Ind	K5 V	3.63	336	−48	22	13,14
HD 201091	61 Cyg A	K5 V	3.48	82	−6	35.4	10,13
HD 26965	40 Eri A	K1 V	5.04	201	−38	37.1	13,14
HD 128621	α Cen B	K0 V	1.35	316	−1	42	13,14

References. — (1) F. C. Fekel 2000, private communication. (2) Cutispoto et al. 1997. (3) Fekel et al. 1986. (4) Jetsu 1993. (5) Hooten & Hall 1990. (6) Bianchi et al. 1991. (7) Mantegazza et al. 1992. (8) Henry et al. 1995. (9) Messina et al. 1999. (10) Donahue et al. 1996. (11) Wichmann et al. 1998. (12) Innis et al. 1988. (13) Gliese & Jahreiss 1991. (14) Saar & Osten 1997.

Table 2. Summary of GHRs Observations

Target	Grating	Aperture	Spectral Range (Å)	Exposure Time (s)	Date	Start Time (UT)	WAVECAL?
HD 220140	G270M	SSA	2775–2822	323	1995 Sept. 22	4:39	No
	G160M	SSA	1202–1240	1185	1995 Sept. 22	5:38	No
HD 1405	G270M	SSA	2775–2822	754	1995 Sept. 29	10:24	No
	G160M	SSA	1202–1240	1293	1995 Sept. 29	10:41	No
HD 197890	G270M	SSA	2775–2822	646	1995 Nov. 7	4:23	Yes
	G160M	SSA	1202–1240	1077	1995 Nov. 7	5:29	No
HD 82443	G270M	SSA	2775–2822	233	1995 Nov. 9	13:05	Yes
	G160M	SSA	1202–1240	1293	1995 Nov. 9	13:27	No
HD 17925	G270M	SSA	2775–2822	431	1996 Jan. 9	4:18	Yes
	G160M	SSA	1202–1240	1077	1996 Jan. 9	4:31	No
HD 82558	G270M	SSA	2775–2822	323	1996 May 4	8:07	Yes
	G160M	SSA	1202–1240	754	1996 May 4	8:19	No

Table 3. Measured ISM Properties^a

Star	Component	V_{Mg} (km s ^{−1})	b_{Mg} (km s ^{−1})	$\log N_{\text{Mg}}$	V_{H} (km s ^{−1})	b_{H} (km s ^{−1})	$\log N_{\text{H}}$	$D(\text{Mg})$
HD 197890	1	-23 ± 2	4.4 ± 1.4	13.80 ± 0.70	-27 ± 3	13.7 ± 1.5	18.30 ± 0.15	...
	2	0 ± 1	3.6 ± 1.5	12.50 ± 0.30	(−4)	(13.7)	(17.00)	...
	totals	13.80 ± 0.70	18.30 ± 0.15	-0.09 ± 0.72
HD 82558	1	6 ± 2	3.2 ± 0.7	12.90 ± 0.25	7 ± 2	10.0 ± 5.0	18.75 ± 0.15	...
	2	14 ± 2	(3.2)	12.90 ± 0.25	(15)	(10.0)	(18.75)	...
	totals	13.20 ± 0.15	19.05 ± 0.15	-1.44 ± 0.21
HD 1405	LIC	10 ± 2	2.5 ± 0.6	13.10 ± 0.50	7 ± 2	13.9 ± 1.2	18.05 ± 0.10	...
	2	2 ± 2	(2.5)	13.10 ± 0.50	(−1)	(13.9)	(18.05)	...
	totals	13.40 ± 0.30	18.35 ± 0.10	-0.54 ± 0.32
HD 220140	LIC	5 ± 1	2.7 ± 0.3	12.70 ± 0.10	7 ± 1	14.2 ± 0.5	17.95 ± 0.10	-0.84 ± 0.14
HD 82443	LIC	11 ± 1	3.0 ± 1.0	12.40 ± 0.10	11 ± 1	12.0 ± 0.5	17.70 ± 0.15	-0.89 ± 0.18
HD 17925	LIC	19 ± 1	3.4 ± 1.0	13.00 ± 0.40	20 ± 1	11.8 ± 0.8	17.95 ± 0.10	...
	2	9 ± 2	(3.4)	12.50 ± 0.30	(10)	(11.8)	(17.45)	...
	totals	13.10 ± 0.30	18.05 ± 0.10	-0.54 ± 0.32

^aQuantities in parentheses are not free parameters of the fit (see text).

Table 4. Predicted ISM Properties

Star	V(LIC) (km s ⁻¹)	V(G) (km s ⁻¹)	log $N_{\text{H}}(\text{LIC})^{\text{a}}$
HD 197890	−14.9	−15.2	16.53
HD 82558	7.9	7.2	16.89
HD 1405	10.5	13.4	18.02
HD 220140	6.9	7.7	17.98
HD 82443	11.3	10.9	17.59
HD 17925	19.1	23.1	17.91

^aPredicted column density from Redfield & Linsky (2000).

Table 5. Chromospheric Line Fluxes

Star	Fluxes (10^{-12} ergs cm $^{-2}$ s $^{-1}$)			% Errors		References
	Mg II k	Mg II h	Lyman- α	Mg II	Lyman- α	
Primary Sample						
HD 197890	0.91	0.73	1.85	5	15	1
HD 82558	2.83	2.27	4.01	5	40	1
HD 1405	1.42	1.12	2.31	3	25	1
HD 220140	3.07	2.45	2.99	3	25	1
HD 82443	3.29	2.58	2.31	4	20	1
HD 17925	7.57	5.83	6.05	8	25	1
Additional Stars						
HD 36705	5.97	4.79	...	5	...	2
HD 22049	48.8	...	25	3
HD 155886	6.39	4.60	14.2	4	20	4
HD 209100	31.0	...	20	5
HD 201091	8.32	5.84	17.2	3	20	6
HD 26965	6.71	4.91	6.93	4	15	6
HD 128621	164	121	150	4	25	7

References. — (1) This paper. (2) Brandt et al. 2000. (3) Dring et al. 1997. (4) Wood et al. 2000. (5) Wood et al. 1996b. (6) Wood & Linsky 1998. (7) Linsky & Wood 1996.

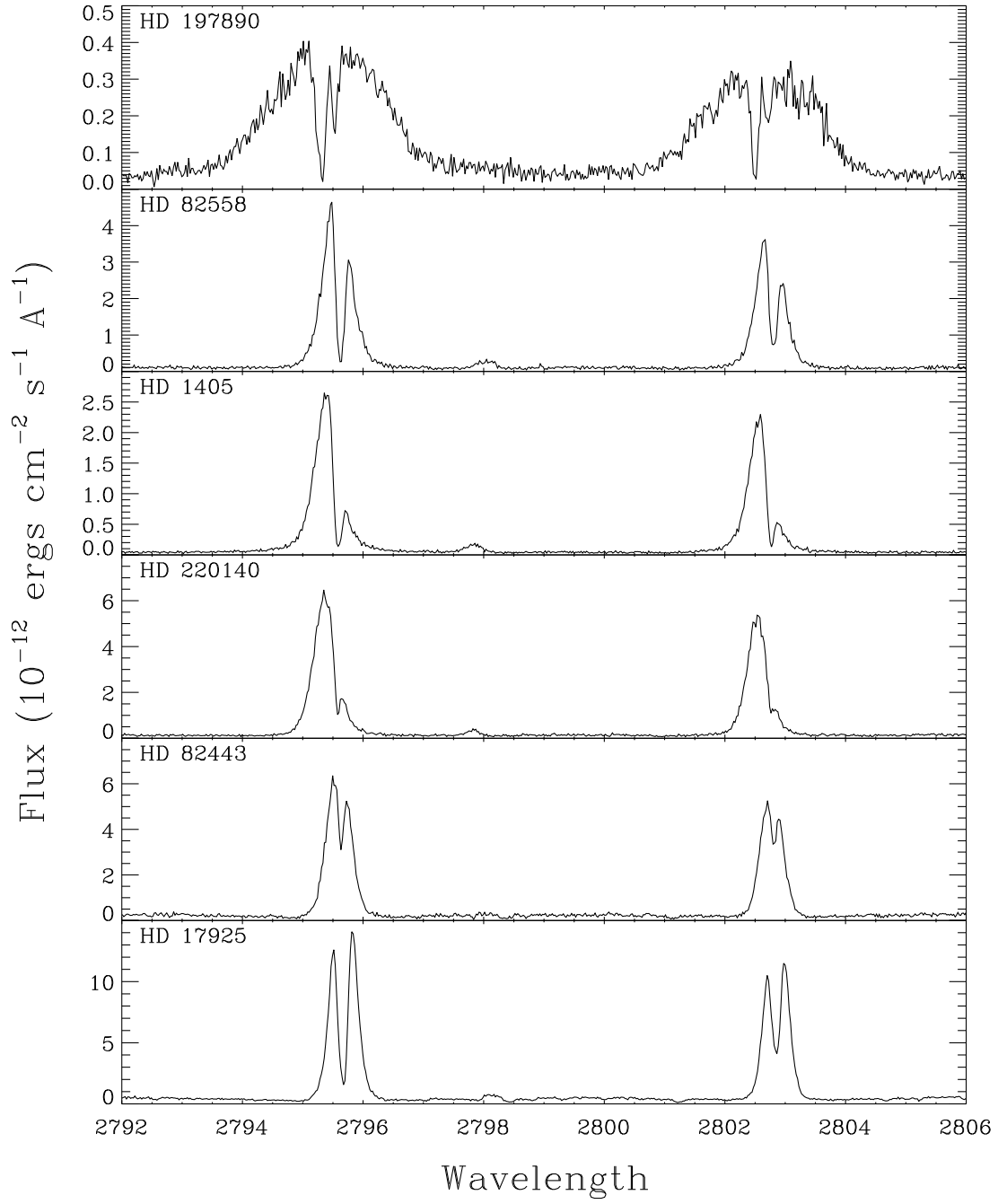


Fig. 1.— The Mg II h & k lines of the six K dwarfs, with rest wavelengths in air of 2802.705 Å and 2795.528 Å, respectively.

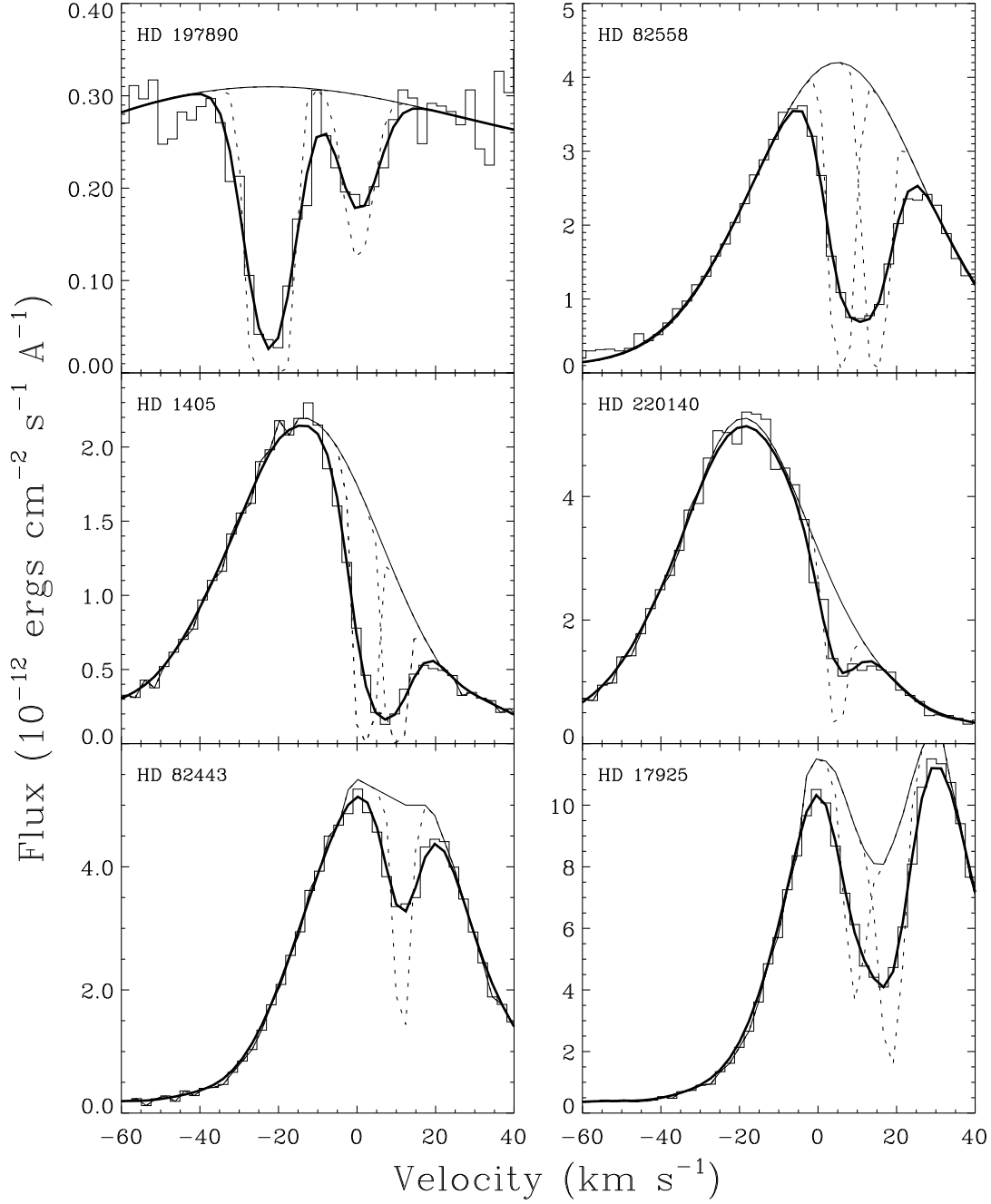


Fig. 2.— Fits to the interstellar absorption observed in the Mg II h lines of the six K dwarf stars. For each star, the assumed stellar emission profile is a thin solid line, the fitted absorption line or lines are dotted lines, and the convolution of these absorption lines with the instrumental profile is the thick solid line, which fits the data.

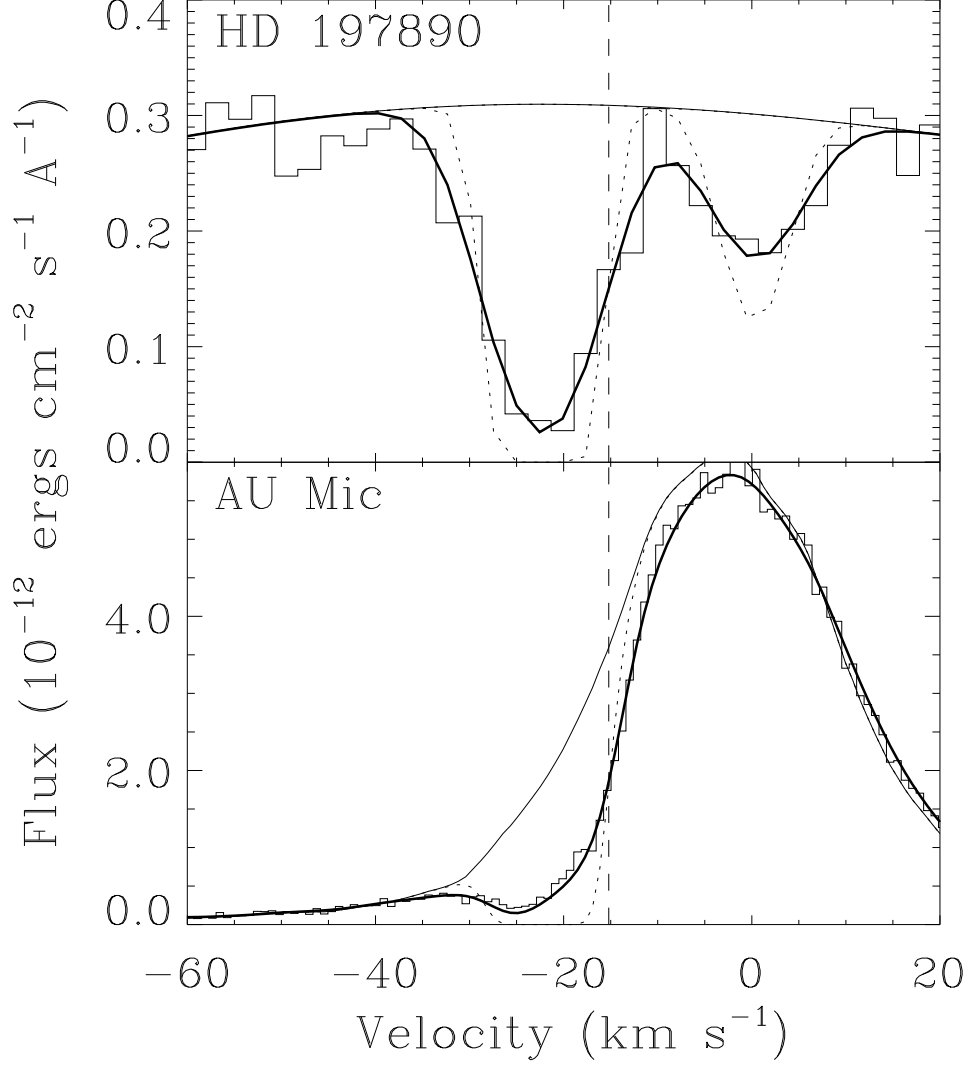


Fig. 3.— The upper panel is a reproduction of the Mg II h line fit to two absorption components of HD 197890 from Fig. 2, and in the bottom panel the fitted absorption profile for the blue component is applied to observations of the Mg II h line of AU Mic, which is only 5° from HD 197890. The same absorption profile fits the absorption of both stars quite well. The red absorption component seen toward HD 197890 is not seen at all toward the closer star AU Mic.

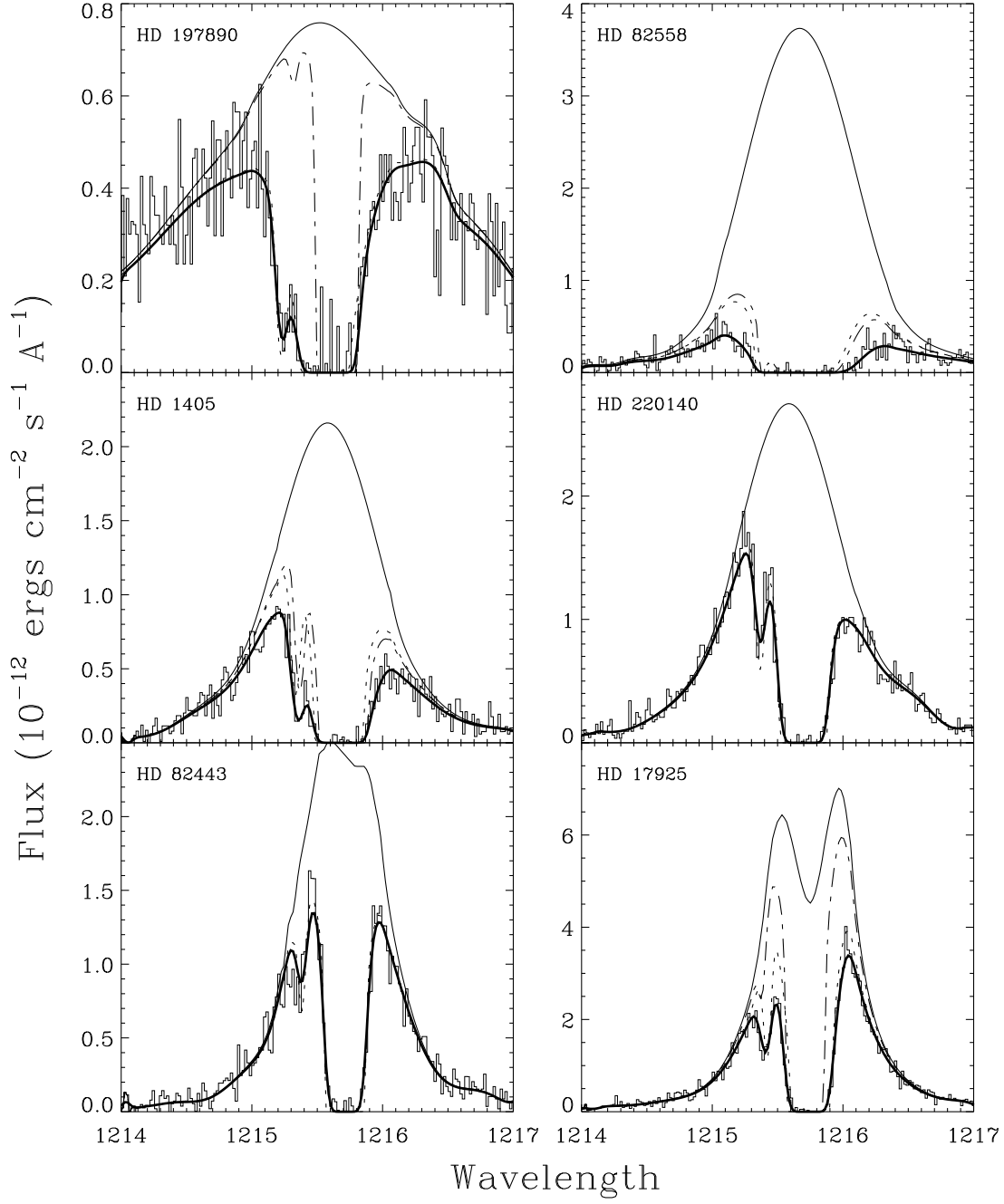


Fig. 4.— Fits to the interstellar hydrogen (H I) and deuterium (D I) absorption observed in the Lyman- α lines of the six K dwarf stars, where the D I absorption is the narrow absorption seen blueward of the broad, optically thick H I absorption. For each star, the assumed stellar emission profile is a thin solid line, the first fitted absorption component is a dotted line, the second absorption component (if there is one) is a dot-dashed line, and the convolution of these absorption components with the instrumental profile is the thick solid line, which fits the data.